
VARIABILITY OF IONOSPHERIC IONIZATION OVER EURASIA ACCORDING TO DATA FROM A HIGH-LATITUDE IONOSONDE CHAIN DURING EXTREME MAGNETIC STORMS IN 2015

M.A. Chernigovskaya 
Institute of Solar-Terrestrial Physics SB RAS,
Irkutsk, Russia, cher@iszf.irk.ru

A.G. Setov
Institute of Solar-Terrestrial Physics SB RAS,
Irkutsk, Russia, setov@iszf.irk.ru

K.G. Ratovsky 
Institute of Solar-Terrestrial Physics SB RAS,
Irkutsk, Russia, ratovsky@iszf.irk.ru

A.S. Kalishin 
Arctic and Antarctic Research Institute,
St. Petersburg, Russia, askalishin@aari.ru

A.E. Stepanov
Institute of Cosmophysical Research and Aeronomy
SB RAS,
Yakutsk, Russia, a_e_stepanov@ikfia.sbras.ru

Abstract. We have examined longitudinal-temporal variations in ionospheric parameters over Eurasia by analyzing data from a chain of high-latitude ionosondes along a latitude circle $\sim 70^\circ$ N (geomagnetic latitudes $58^\circ < Glat < 65^\circ$) in the longitudinal sector $26\text{--}171^\circ$ E during severe magnetic storms of solar cycle 24 in March and June 2015. To analyze the response of ionospheric ionization to geomagnetic disturbances, we have used ionosonde data on hourly average critical frequency f_oF_2 of the ionospheric F2 layer. Strong differences were observed between common peculiarities of temporal variations in f_oF_2 for the analyzed periods of magnetic storms, which are likely associated with the characteristic features of the seasonal and diurnal variations in the background high-latitude ionosphere of the given geographic region. During the main and early recovery phases of magnetic storms there were periods of blackouts of ionosonde radio signals. Differences in the character of the ionospheric response to geomagnetic dis-

turbances have been noted. This is probably due to seasonal features of the probability of occurrence of the ionospheric storm positive or negative phase in different seasons of the year. The trends of increasing ionospheric ionization over the vast region of Eastern, Western Siberia and Europe after the end of the extreme magnetic storm in March 2015, according to measurements from the chain of high-latitude ionosondes, may be associated with the formation of an area of increased [O]/[N₂] ratio over this territory. Such an increase in ionospheric ionization exceeding the background level of f_oF_2 values can be considered as a clear manifestation of the after-effect of magnetic storms.

Keywords: high-latitude ionosphere; ionosonde chain, geomagnetic storm, variations of ionospheric ionization.

INTRODUCTION

The research focuses on variations in the parameters characterizing the state of the high-latitude ionosphere during severe magnetic storms of solar cycle 24 in March and June 2015. According to the classification by Hunsucker and Hargreaves [2003], which divides the ionosphere into latitudinal zones with significantly different properties depending on geomagnetic latitude, by high-latitude ionosphere we mean the region above 60° geomagnetic latitude (*Glat*). This region includes the subauroral ionosphere adjacent to it from midlatitudes ($55^\circ < Glat < 65^\circ$) [Mamrukov et al., 2000], the auroral ionosphere ($65^\circ < Glat < 75^\circ$), and the polar cap ($Glat > 75^\circ$).

The study of the nonstationary and inhomogeneity structure of the high-latitude ionosphere is of particular fundamental importance for understanding physics of ionospheric processes under quiet and disturbed geomagnetic conditions, as well as for practical problems of ensuring stable radio communications and navigation in polar regions.

The high-latitude ionosphere has a complex spatial structure determined by its close relationship with Earth's magnetosphere and the processes occurring in it. Precipitation of high-energy charged particles from the magnetosphere into the ionosphere, intense electric fields and currents are among the main mechanisms for the formation of various structural features and inhomogeneities in the large-scale structure of the high-latitude ionosphere. From ground-based and satellite sounding data, the following structural features of the high-latitude ionosphere have been identified: ionospheric ionization troughs (main, narrow, ring, high-latitude, etc.), polar and auroral ionization peaks, polar cavity, ionization tongue [Krinberg, Tashilin, 1984; Deminov, 2015; Stepanov et al., 2017; Tumanova et al., 2016; Deminov, Shubin, 2018; Karpachev et al., 2019; Karpachev, 2021]. All these structural features have characteristic spatial and temporal peculiarities of formation, depend on heliogeomagnetic activity, season, time of day, and geographical location of the observation site. They are most clearly manifested in winter or at night, even under quiet geomagnetic conditions. In

summer when most high-latitude ionosphere is sunlit during the polar day, these features are smoothed out or absent at all. The ionization troughs localized under quiet conditions in narrow latitudinal regions expand and shift toward midlatitudes during increased geomagnetic activity. In high latitudes, neutral winds are induced which redistribute the neutral composition of the atmosphere over most of the high-latitude region and part of the mid-latitude region, causing eventually the ionospheric plasma ionization to change.

In ionospheric physics, as well as in near-Earth space physics as a whole, the tools for acquiring knowledge are remote measurements (ground and satellite) along with simulation results. To date, there is no detailed model description of variations in the spatio-temporal distribution of plasma parameters in the high-latitude ionosphere. First of all, this is due to the difficulty in modeling ionospheric irregularities. Another reason is related to the limited experimental ionospheric database in high latitudes, which does not allow us to improve the quality and accuracy of empirical and semi-empirical models of the high-latitude ionosphere, as well as to adequately verify theoretical models.

A successful example of the constantly improving model of the high-latitude ionosphere, designed to replace IRI in high latitudes, is the Empirical Canadian High Arctic Ionospheric Model (E-CHAIM) [Themens et al., 2017]. It simulates the peak characteristics of the ionosphere for geomagnetic latitudes above 50° N: N_mF2 and h_mF2 for quiet conditions and N_mF2 for disturbed conditions. Three real geomagnetic indices are used to describe geomagnetic conditions: Dst , A_p , AE , integrated from the World Data Center (WDC) for Geomagnetism, Kyoto [<http://wdc.kugi.kyoto-u.ac.jp/>] (Dst and AE), as well as the National Geophysical Data Center (NOAA NGDC) [<https://www.ngdc.noaa.gov/>] (A_p), which provides a higher accuracy of the model as compared to traditional ones.

The number of ground-based observation stations in polar regions is severely limited for obvious reasons (high cost, inaccessibility, harsh climate, huge water areas, etc.). In recent decades, satellite remote sensing methods have been widely used to study spatial-temporal characteristics of the ionosphere. In radio occultation and tomographic measurements, radio signals passing through the ionosphere from satellites, which make up constellations of low- and high-orbit satellite systems, are extensively employed to examine ionospheric conditions [Jakowski, 2005; Alpatov et al., 2013; Kunitsyn et al., 2016; Andreeva et al., 2021]. The most common application of the Global Navigation Satellite System (GNSS) satellites (GPS, GLONASS, Beidou, Galileo, etc.) was to use their signals to calculate the parameter characterizing the total electron content (TEC) of the ionosphere [Afraimovich, Perevalova, 2006; Afraimovich et al., 2013; Cherniak et al., 2014]. Monitoring with high-orbit navigation satellites provides wide coverage of the territory and observation in remote and hard-to-reach areas, including high-latitude ones [Perevalova et al., 2020], but even in the case of GNSS satellites there are problems and limitations of

their use in high latitudes. They chiefly concern the inclination of orbits of navigation satellites. The GPS and Beidou satellites have an orbital inclination $\sim 55^\circ$ to the equator; Galileo and GLONASS have higher orbital inclinations of 56° and 64.8° respectively. At latitudes above the Arctic Circle ($\sim 66.5^\circ$), several navigation satellites are visible at any given time due to their high orbit (~ 20 thousand km), but they never pass right overhead. A large error in the accuracy of the navigation systems is introduced by the environment in which the satellite radio signal propagates. The ionization irregularities of different scales in the high-latitude ionosphere associated with manifestations of heliogeomagnetic or meteorological activity cause fluctuations in the amplitude and phase of GNSS satellite signals, thereby ultimately reducing the positioning and timing accuracy [Afraimovich, Perevalova, 2006]. This is especially true of the Arctic and Antarctic regions, where space weather largely determines the state of the polar ionosphere affecting propagation of satellite radio signals.

Recently, the use of small spacecraft, including nanosatellites weighing from 1 to 10 kg, for example, the CubeSat standard [Chernyshov et al., 2016], for commercial, research, and educational purposes is considered a promising direction. The success of CubeSat was ensured by their unification and standardization. Since the cost of launching a space satellite primarily depends on weight, light small-sized nanosatellites have a great advantage over medium and large satellites. From such small devices, it is possible to make a large constellation of satellite systems whose work will be coordinated, but individual devices will perform individual tasks.

The insufficiency of experimental ionospheric database in high latitudes as well as models that can adequately reproduce variations in the parameters of the high-latitude ionosphere causes difficulties in predicting radio wave propagation. This primarily defines the practical significance of the research into the high-latitude ionosphere — the need to ensure the reliability of radio communications and navigation in polar regions. Radio communication conditions depend on three main factors: height of ionospheric layers, vertical distribution of concentration of free electrons, and degree of radio wave absorption. All these parameters can be determined by vertical sounding (VS) of the ionosphere by ionosondes. Scanning by sounding radio pulses in different frequencies yields height-frequency characteristics of the ionosphere (ionograms) from which we can then obtain vertical distribution of electron density up to the F2-layer maximum ionization height.

At previous stages of the studies based on data from the Eurasian mid-latitude ionosonde chain, as well as from mid- and high-latitude chains of GPS/GLONASS receivers and INTERMAGNET magnetometers, the longitude features of the ionospheric response to the extreme magnetic storms in March and June 2015 [Chernigovskaya et al., 2019, 2020; Chernigovskaya et al., 2021] as well as to a series of magnetic storms in March 2012 [Chernigovskaya et al., 2022, 2023] were analyzed.

For a comprehensive study of spatial-temporal features of ionospheric irregularities from radiophysical measurement data, to the analysis we add measurement data from the chain of high-latitude ionosondes located in the north of the Eurasian continent at the latitude of the Arctic Circle and at higher latitudes. Simultaneous analysis of measurement data from the mid- and high-latitude ionosonde chains allows us to explore the global nature of spatio-temporal variations in ionospheric parameters over the Eurasian region, to analyze the similarities and differences in the reaction of the mid- and high-latitude ionosphere to changes in external (heliogeomagnetic activity) and internal (variations in the main geomagnetic field) factors affecting the state of ionospheric plasma. Studying temporal variations in longitude-latitude distributions of ionization parameters over the Eurasian region of interest will enable us to examine movements of ionospheric ionization troughs from high latitudes to middle latitudes during magnetic storms. Thus, this work is a logical and very relevant sequel to our previous studies of the spatio-temporal variations in the ionosphere over Eurasia.

ANALYSIS OF HELIOGEOMAGNETIC CONDITIONS

Features of the strongest magnetic storms of solar cycle 24 in March and June 2015 have been analyzed in detail in [Chernigovskaya et al., 2019, 2020; Chernigovskaya et al., 2021]. Both magnetic storms were severe (Dst below -200 nT) according to the classification of storms by the Dst planetary index [Loewe, Pröls, 1997]. According to NASA's classification, the storms also belonged to the G4 class [https://www.swpc.noaa.gov/noaa-scales-explanation].

Since this work deals with the heliogeomagnetic effects of the high-latitude ionosphere, in addition to the

geomagnetic indices Dst , K_p , A_p we use the geomagnetic activity indices AE and PCN characterizing magnetic activity in the polar caps (Figure 1). AE measures the magnetic disturbance caused by amplification of currents flowing along the boundary of the auroral oval in the ionosphere (eastward and westward polar electrojets).

PC as a characteristic of magnetic activity in the polar caps was finally formed only in 2006 when a unified procedure for calculating it online was developed from data obtained at the stations Thule in Greenland (PCN) and Vostok in the Antarctic (PCS) [Troshichev, Sormakov, 2018]. The unified PC index measures the strength of the geoeffective interplanetary electric field E_m impacting on the magnetosphere, as well as the solar wind dynamic pressure. Geomagnetic disturbances begin when PC exceeds ~ 2 mV/m, and stop when PC falls below this threshold. The threshold storm levels of Dst and PCN are indicated by red horizontal dashed lines in Figure 1. Vertical dashed lines show the time of the storm onset (labelled S) and the time of magnetic storm intensity maxima (denoted by M).

In March 2015, a magnetic storm began on March 17 (according to the day of onset, the storm was named after St. Patrick). According to the information posted on the website [www.solen.info/solar/ol_d_reports/] and based on data from the SOHO satellite, the storm was caused by the interaction of Earth's magnetosphere with high-speed solar wind streams from four coronal holes (coronal hole high speed streams, CH HSS) and coronal mass ejection (CME) accompanied by a relatively weak X-ray flare of C9.1 class, recorded on March 15, 2015. The storm main phase lasted for ~ 16.5 hrs — from the storm sudden commencement (SSC) at 06:23 UT (line S in Figure 1, a) to 22:47 UT. During the storm maximum, Dst decreased to -223 nT (M1 line, panel a); K_p increased from 5+ to 8+; A_p was as high as 179 according to the data from the website of the World Data Center

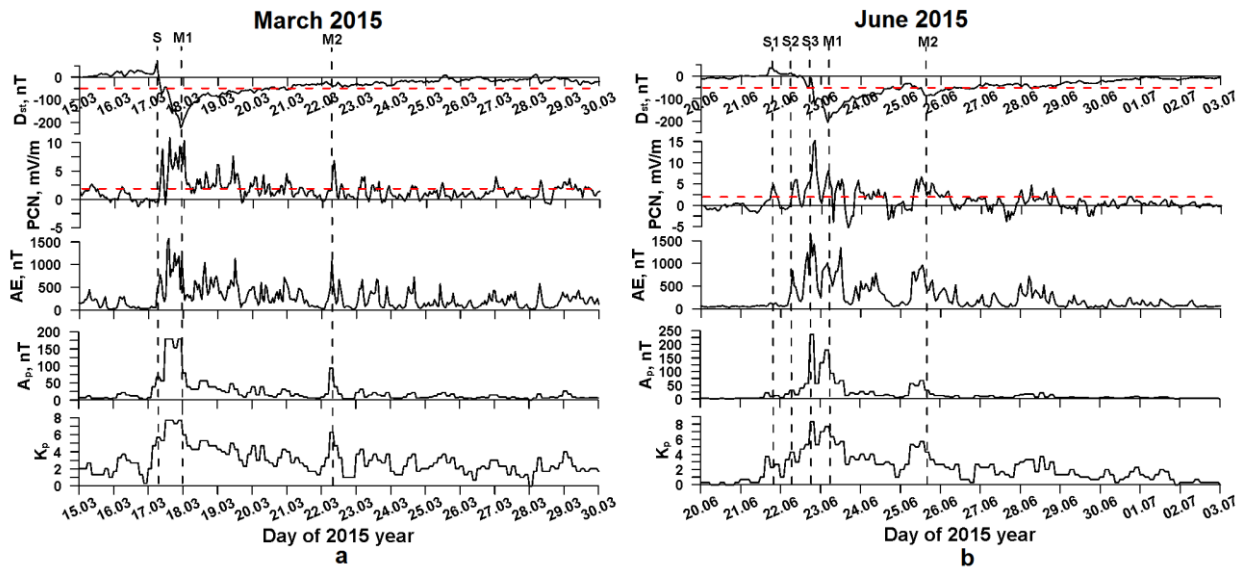


Figure 1. Variations in geomagnetic activity indices during storms in March (a) and June (b) 2015. Vertical dashed lines indicate the time of the storm onset (denoted by S) and intensity maxima (labelled M). Threshold storm levels of the Dst and PCN indices are shown by red horizontal dashed lines.

for Geomagnetism, Kyoto [<https://wdc.kugi.kyoto-u.ac.jp/wdc/Sec3.html>].

Noteworthy is a significant increase in AE [<https://wdc.kugi.kyoto-u.ac.jp/wdc/Sec3.html>] and PCN [http://www.wdcb.ru/stp/geomag/geomagn_PC_ind.ru.html] during the storm main and early recovery phases. It indicates an increase in the solar-wind drivers of the storm [Troshichev, Sormakov, 2018; Kalishin et al., 2020]. The close correlation between PCN and AE amplifications suggests that the interplanetary electric field and the solar wind dynamic pressure had a strong geoeffective impact on Earth's magnetosphere and ionosphere in the polar region. This led to a significant amplification of currents flowing along the auroral oval boundary in the ionosphere — the eastward polar electrojet ($AE > 0$).

An isolated increase in magnetic activity was observed on March 22, 2015 from 06:00–09:00 to ~18 UT. The activity increase was caused by the impact of CH HSS on Earth's magnetosphere. Geomagnetic effects associated with CH HSS events usually have little effect on Dst variations, but are clearly visible in variations in other geomagnetic indices, especially in PCN , AE , A_p , and K_p (K_p increased to 6 $_+$; A_p was as high as 94 (M2 line in panel *a*).

The second most intense magnetic storm of solar cycle 24 resulted from the impact of high-speed solar wind, CMEs, and a series of solar flares on Earth's magnetosphere. The M6/2b flare occurred on June 22, 2015 at 18:23 UT [www.solen.info/solar/old_reports/]. This event was preceded by the effects of the M2/1n flare on June 21 along with numerous CMEs on June 18, 19, and 21. From June 21 to 22, 2015, the fronts of three interplanetary shock waves of different intensity (lines S1, S2, S3 in panel *b*) arrive at Earth. The front of the third, strongest shock wave reached Earth's magnetosphere at 18:30 UT on June 22 (line S3) after which a severe G4 class geomagnetic storm began [Loewe, Pröls, 1997]; it lasted for many hours. During the storm maximum, Dst decreased to -204 nT (M1 line in panel *b*), K_p increased to 8 $_+$, A_p was as high as 236, as derived from [<https://wdc.kugi.kyoto-u.ac.jp/wdc/Sec3.html>].

The arrival of the fronts of three CME-driven inter-

planetary shock waves of different intensity at Earth on June 21–22, 2015 was very clearly reflected by maxima in variations of PCN (lines S1–S3 in panel *a*) and AE . PCN increased during SSC (S3 line) to ~15 mV/m. For comparison, during the most intense magnetic storm in March 2015 PCN was as high as 10 mV/m. This indicates very high geoeffectiveness of the magnetic storm in June 2015.

Later, on June 24, 2015, the CME effect associated with the M6/2b solar flare on June 22 was observed. By June 25, the intensity had increased again to the level of a weak geomagnetic storm — Dst was -86 nT (M2 line in panel *b*), K_p increased to 6 $_+$, A_p was as high as 67. There was also an increase in AE , which indicates an increase in the eastward auroral electrojet during this period. Thus, the period of the June 2015 extreme magnetic storm was very difficult and long-lasting.

EXPERIMENTAL MEASUREMENT DATA

To analyze the spatio-temporal variations in the ionospheric parameters during the extreme geomagnetic disturbances in March and June 2015, we use data on the hourly average maximum electron density and the height of the F2-layer maximum ionization from measurements made at a chain of seven high-latitude ionosondes, located in the latitude range 67° – 71° N (geomagnetic latitudes $58^\circ < Glat < 65^\circ$) in the longitude sector 26 – 171° E of the Eurasian continent (Figure 2, red dots and labels; Table). The chain consists of ionosondes of Russian scientific organizations: ISTP SB RAS, SHICRA SB RAS (DPS-4 in the stations Norilsk and Zhigansk) and AARI Roshydromet (Canadian Advanced Digital Ionosonde, CADI [MacDougall et al., 1995; Vystavnoi et al., 2013; Kalishin et al., 2020] at the stations Lovozero, Amderma, Salekhard, and Pevek). We also employ SO166 ionosonde (Alpha Wolf) data [Kozlovsky et al., 2013; Enell et al., 2016] from the Sodankylä Geophysical Observatory (Finland) [https://www.ukssdc.ac.uk/wdccc1/iono_menu.html].

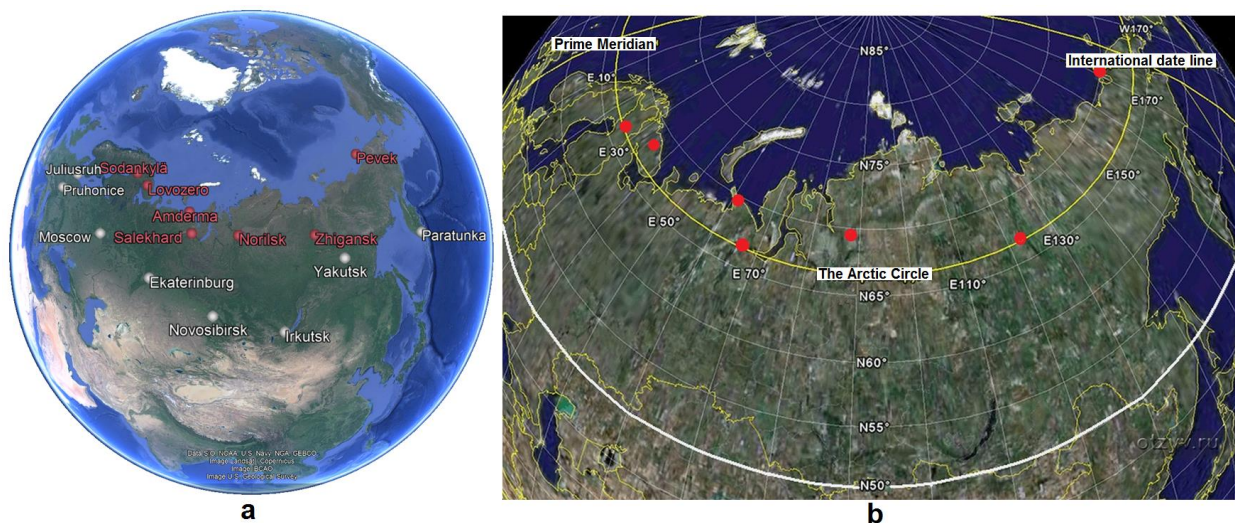


Figure 2. Maps of the location of chains of high- and mid-latitude Eurasian ionosondes (*a*) and ionosondes of the high-latitude chain relative to the Arctic Circle (*b*)

High-latitude ionosondes

Ionosonde	Ionosonde type	Geographic coordinates		Geomagnetic coordinates	
		Latitude	Longitude	Latitude	Longitude
Sodankylä	SO166	67° N	26° E	64° N	118° E
Lovozero	CADI	68° N	35° E	64° N	126° E
Amderma	CADI	70° N	61° E	63° N	147° E
Salekhard	CADI	67° N	67° E	59° N	150° E
Norilsk	DPS-4	69° N	88° E	60° N	166° E
Zhigansk	DPS-4	67° N	123° E	58° N	169° W
Pevek	CADI	71° N	171° E	65° N	135° W

Historically, it took great organizational efforts and serious material resources to create such a longitudinally distributed network of high-latitude stations on the territory of Russia. The first studies of the high-latitude ionosphere were conducted at the station in Tikhaya Bay (Franz Josef Archipelago) since 1939 [Vystavnoi et al., 2013]. All these problems were successfully solved by scientists of AARI Roshydromet. Currently, a network of digital ionospheric stations has been built up at high latitudes with online transmission of main ionospheric parameters to the Single Data Center for subsequent processing and prediction of the background state of the auroral ionosphere. This ionospheric VS network allows continuous monitoring of fast processes in the

high-latitude ionosphere [Kalishin et al., 2020].

By mutual agreement between the study participants, all ionograms on the analyzed dates have been manually processed to minimize possible errors during automated ionogram processing. As in previous studies based on measurement data from the mid-latitude ionosonde chain [Chernigovskaya et al., 2019, 2022; Chernigovskaya et al., 2021], we use the F2-layer critical frequency f_oF2 to analyze ionospheric effects of magnetic storms, which is proportional to the F2-layer maximum electron density N_mF2 [Polyakov et al., 1968], and the height of the F2-layer maximum ionization h_mF2 , determined from the minimum equivalent heights $h'F$ and $h'F2$ obtained from VS ionograms (Figure 3).

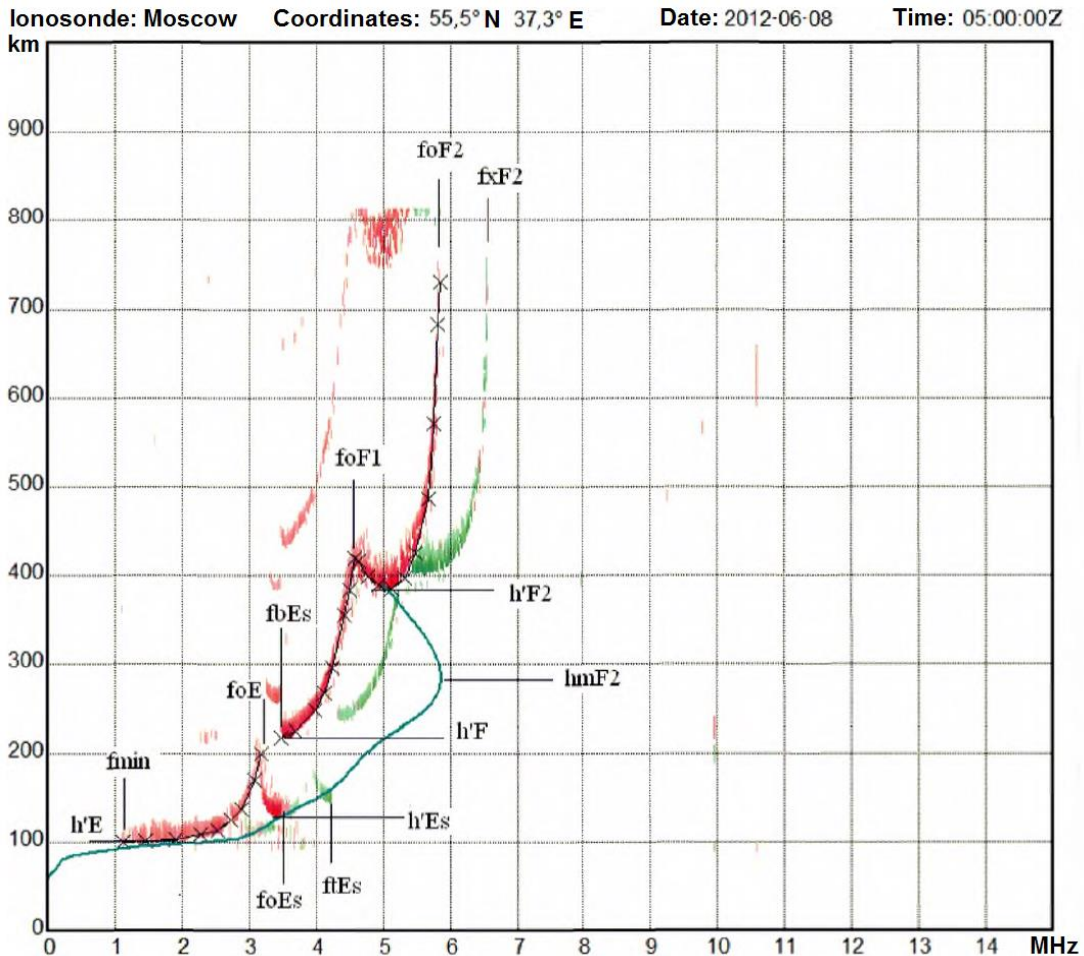


Figure 3. A vertical sounding ionogram [http://icenter.izmiran.ru/f-h_db.php]

Figure 3 exemplifies the operation of a VS ionosonde — ionograms with characteristic traces of reflections of high-frequency pulsed radio signals generated by ionosondes (from the website [http://icenter.izmiran.ru/f-h_db.php/], where the ionospheric characteristics determined from the VS ionograms are also described in detail). An ionogram in the form of a height-frequency characteristic represents the dependence of the equivalent reflection height (or the time it takes for a radio signal to reach a reflection point and return back) on the operating frequency of the ionosonde. The characteristic minimum equivalent heights $h'E$, $h'F$, $h'F2$, as well as the critical frequencies f_oE , f_oF1 , f_oF2 for each layer are determined from ionograms manually or automatically, using special computer programs. The main target parameters are N_mF2 and h_mF2 . They are calculated by programs developed individually for ionosondes of different types with due regard to their technical characteristics and methodological recommendations for recalculating the standard ionospheric parameters from VS ionograms.

In the present study, in the analysis of variations in ionospheric parameters from data obtained at the chain of high-latitude CADI ionosondes in Pevek, Salekhard, Amderma, and Lovozero (see Figure 2 and Table) there is no data on h_mF2 since there is no program for standard processing of ionogram parameters for CADI ionosondes. We have, therefore, carried out an additional study based on DPS-4 measurements in Irkutsk and Norilsk to clarify the features of variations in the following parameters (see the example in Figure 3): (1) $h'F2$ (or $h'F$ if there is no F1 layer) — the standard parameter obtained from VS ionograms and (2) h_mF2 — a parameter calculated from ionograms, using a software package for interactive ionogram processing by the method from [Huang, Reinisch, 1996]. Comparative analysis of temporal variations in h_mF2 (black curves in

Figure 4) and $h'F2$ (gray curves in Figure 4) for the magnetic storms in March and June 2015 (see Figure 1) has shown the following.

1. Under quiet conditions on March 15–16, 2015 (Figure 4, *a, b*) and June 20–21, 2015 (*c, d*), both heights generally have a similar diurnal variations with a minimum near noon (12 LT) and a maximum near or after midnight (00–04 LT). In general, $h_mF2 > h'F2$. For equinox conditions, the mean excess is ~ 32 km (*a, b*); the daily average (10–14 LT), ~ 27 km, and the nighttime average (00–04 LT), ~ 33 km. For the summer solstice, the mean excess is ~ 50 km (*c, d*); the daily average (10–14 LT), ~ 60 km; and the nighttime average (00–04 LT), ~ 40 km. Under quiet conditions, $h'F2$ increases are also observed in Norilsk on March 16, 2015 (*a*) and June 20, 2015 (*c*) and in Irkutsk on June 21, 2015 (*d*); they exceeded h_mF2 at the same local time.

2. During magnetic storms, the quiet day conditions are significantly violated. In the high-latitude ionosphere over Norilsk, the time interval of irregular variations when a strong ionospheric storm is clearly seen, is much longer (Figure 4, *a, c*) than in the mid-latitude ionosphere over Irkutsk (*b, d*). According to Norilsk ionosonde data on variations in the F2-layer heights in March 2015, the ionospheric storm lasted from March 17 to March 21, 2015 (*a*); and according to Irkutsk ionosonde data, from March 17 to March 18, 2015 (*b*). For the magnetic storm in June 2015, the ionospheric storm, according to the Norilsk ionosonde data, lasted from June 22 to June 26, 2015 (*c*); and according to the Irkutsk ionosonde data, from June 22 to June 23, 2015 (*d*). During the main and early recovery phases of the magnetic storms, there were periods of complete absence of VS data because of radio signal blackouts (gray rectangles).

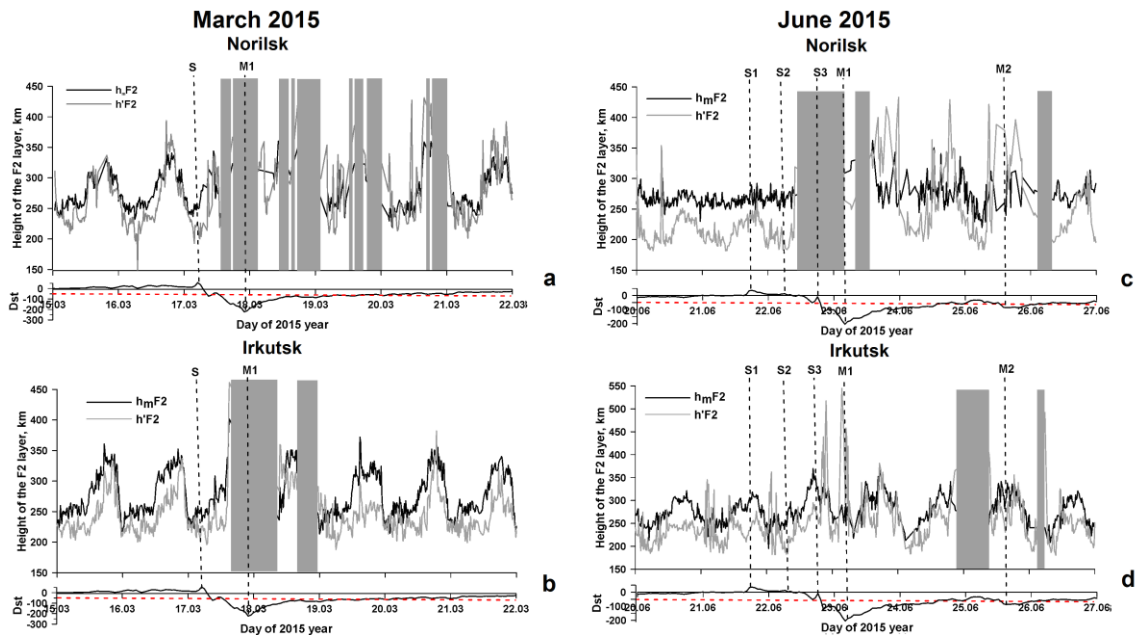


Figure 4. Temporal variations in h_mF2 (black curves), $h'F2$ (gray curves), according to data from DPS-4 digisondes in March 2015 (*a* — Norilsk, *b* — Irkutsk) and June 2015 (*c* — Norilsk, *d* — Irkutsk), and in Dst . The time is in UT. Gray rectangles represent periods of radio signal blackouts. Vertical dashed lines are the time of the storm onset (denoted by S) and the intensity maxima (labelled M)

Thus, Figure 4 shows that during strong magnetic storms $h'F2$ varies chaotically and often significantly (up to 100 km) exceeds h_mF2 . This excess is attributed to the phenomenon called G-conditions when $f_oF1 \geq f_oF2$; in this case, h_mF2 being the height of maximum in fact represents h_mF1 .

Even such a simple comparative analysis gives grounds to conclude that it is impossible to use simultaneously h_mF2 and $h'F2$ during increased geomagnetic activity. They are uncorrelated, there is no linear relationship between them, and their variations are irregular. In this case, it is impossible to model a correction factor that would reduce the sample of these different values to a homogeneous one suitable for simultaneous analysis of spatio-temporal variations in the parameter characterizing variations in the height of the ionospheric ionization maximum. In what follows, therefore, to comparatively analyze variations in ionospheric parameters during magnetic storms obtained from measurements made at chains of mid- and high-latitude ionosondes (see Figure 2), we use only the parameter f_oF2 .

RESULTS OF ANALYSIS OF EXPERIMENTAL DATA ON HIGH-LATITUDE IONOSPHERE IONIZATION OVER EURASIA

During magnetic storms, a broad range of processes develops in ionospheric plasma in response to geomag-

netic effects (ionospheric storms). The storms cause ionospheric parameters to change significantly. For example, during disturbed periods f_oF2 can decrease or increase compared to values under quiet conditions (negative or positive ionospheric storms respectively) [Matsushita, 1959; Buonsanto, 1999; Mikhailov, 2000].

Figure 5 exhibits temporal variations in f_oF2 according to measurements of the high-latitude chain of Eurasian ionosondes for March 15–30, 2015 (a) and June 20 – July 02, 2015 (b). Bottom panels in Figure 5, a, b show Dst variations during magnetic storms. Red dashed lines indicate the level of $Dst = -50$ nT, when, according to the classification from [Loewe, Prölss, 1997], the conditions of geomagnetic activity are classified as stormy (weak magnetic storm). Vertical black dashed lines correspond to the designations in the plots presented in Figure 1. They denote the time of the storm sudden commencement (S) and the time of the maximum intensity of the magnetic storm (M). Unfortunately, during the storm in March 2015, the ionosonde in Amderma did not work for technical reasons. It was deployed on March 21, 2015 at 13:55 UT (see Figure 5, a). Black solid horizontal lines show daily average levels of f_oF2 calculated from 14 quiet days before the storms.

Red solid horizontal lines indicate linear trends of temporal variations in f_oF2 .

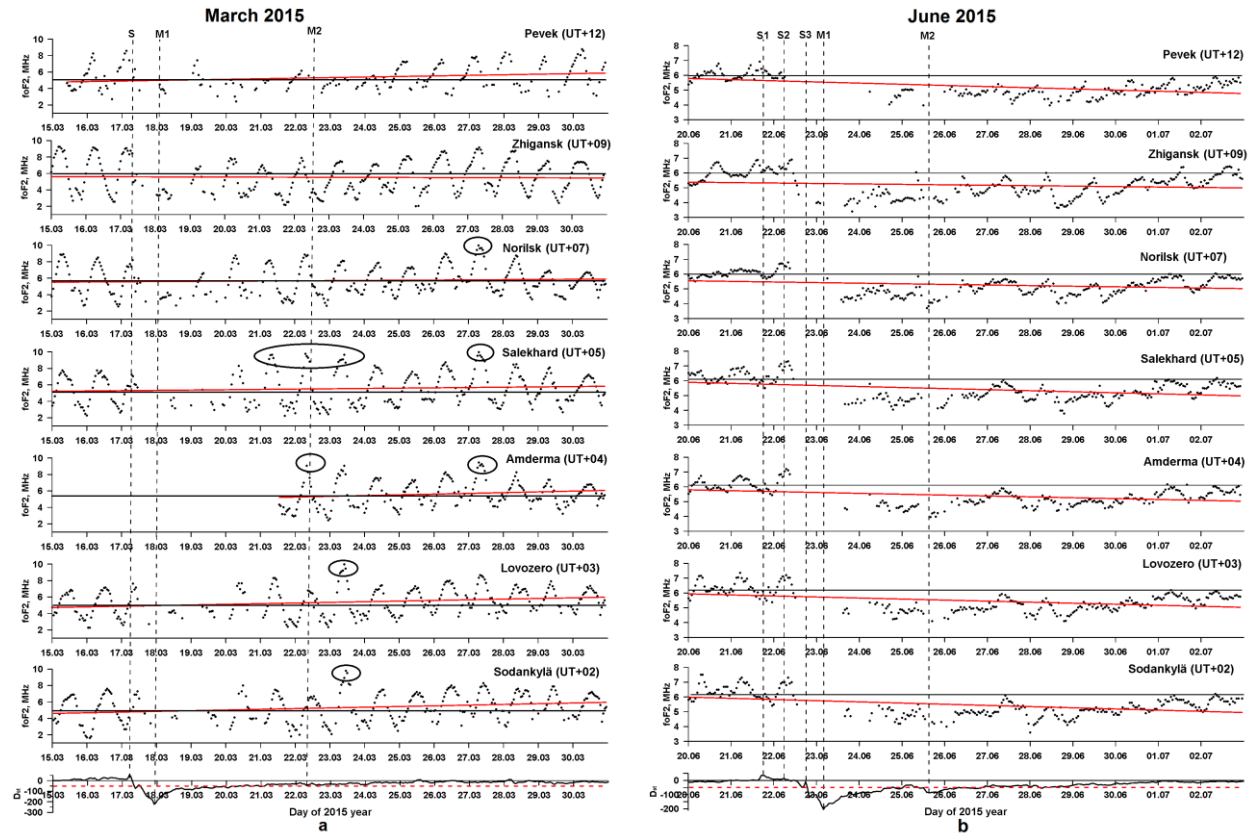


Figure 5. Temporal variations in f_oF2 (black dots) according to measurements of high-latitude ionosondes and Dst variations for magnetic storms in March (a) and June (b) 2015. The time is in UT. Vertical dashed lines indicate the time of the storm onset (S) and the time of intensity maxima of the magnetic storms (M). Black solid horizontal lines are daily average levels of f_oF2 calculated from 14 quiet days before the storms. Red solid horizontal lines are linear trends of temporal variations in f_oF2

Plots in Figure 6 represent the f_oF2 variations, but in more detail on an enlarged scale for March 16–19, 2015 (Figure 6, *a*) and June 20–26, 2015 (Figure 6, *b*). In addition, gray rectangles mark the periods of ionosonde radio signal blackouts as in the plots of Figure 4.

Noteworthy are the large differences in the nature of temporal variations in f_oF2 for the analyzed magnetic storms. Obviously, these differences are due to the fact that the storms occurred in different seasons — March (the period of the vernal equinox) and June (the period of the summer solstice). Therefore, the background characteristics of the ionosphere peculiar to quiet geomagnetic conditions manifest their seasonal and diurnal features [Ratovsky et al., 2013].

1) The diurnal peak-to-peak amplitude of f_oF2 variations (the difference between maximum and minimum diurnal variations) differs significantly on quiet days before onsets of the magnetic storms and on subsequent disturbed days for the equinox (Figure 5, *a*) and the solstice (Figure 5, *b*). Different seasons of the year are characterized by different features of regular variations in the ionosphere, for example, diurnal ones. During the summer solstice, the regions, where ionosondes of the

high-latitude chain are located, are in the conditions of the polar day when the Sun does not set below the horizon almost all day. In spring, diurnal variations in f_oF2 are significantly higher than in summer. The peak-to-peak amplitude of the f_oF2 variations in March 2015 was 5–6 MHz (Figures 5, *a*, 6, *a*); in June 2015, 2–3 MHz (Figures 5, *b*, 6, *b*).

2) After onsets of the magnetic storms (lines S in Figures 5, *a, b* and 6, *a, b*) during the storms' main phases (up to lines M1 in Figures 5, *a, b* and 6, *a, b*), there are long data gaps.

The complete absence of traces of reflections of radio signals, generated by ionosondes, in ionograms results from the combined action of the mechanisms of ionization decrease in the upper ionosphere (negative ionospheric storms are the dominant characteristic in the ionospheric response to increasing geomagnetic activity) and an abnormal increase in the absorption of radio waves in the lower ionosphere. This is because during geomagnetic disturbances the ionization of the lower ionosphere (D-region) is often very high due to precipitation of energetic particles from the magnetosphere

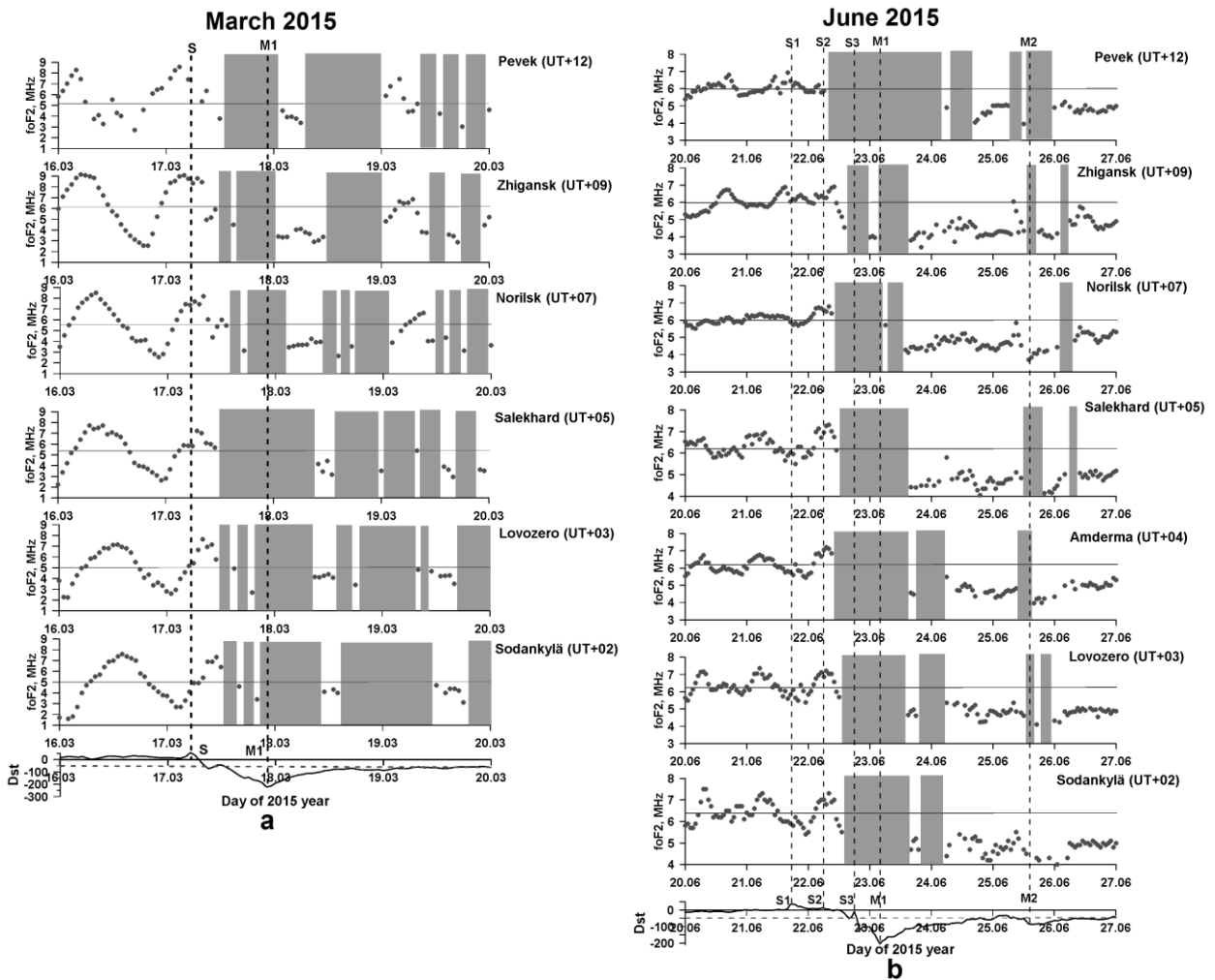


Figure 6. Temporal variations in f_oF2 (black dots) according to measurements of high-latitude ionosondes and in Dst for the magnetic storms in March (*a*) and June (*b*) 2015. The time is in UT. Black solid horizontal lines are daily average levels of f_oF2 calculated from 14 quiet days before the storms. Gray rectangles represent periods of radio signal blackouts. Vertical dashed lines are the time of the storm onset (S) and intensity maxima (M)

along magnetic field lines into the high-latitude ionosphere. As a result, mid- and high-frequency radio waves, employed for VS, are completely absorbed in the lower ionosphere. This phenomenon is called a blackout and seriously hinders ionospheric observations by traditional methods, in particular, with vertical and oblique sounding.

For a more detailed analysis of the effects of magnetic storms in ionospheric ionization, it is necessary to additionally examine variations in f_{\min} characterizing radio wave absorption in the lower ionosphere in the D-region [Chernigovskaya et al., 2024], as well as f_oE_s , describing the formation of the blanketing sporadic layer E_s in the ionospheric E-region, which is the task of the follow-up extensive study.

In March 2015, according to the data from the ionosondes in Norilsk, Lovozero, and Sodankylä with short intervals of blackouts, it is still possible to trace the diurnal variation of f_oF2 in the main phase of the March 17, 2015 storm (Figure 6, *a*). According to the data from the ionosondes in Pevek, Zhigansk, and Salekhard, complete blackouts of radio signals were observed from the late afternoon on March 17, 2015 (*a*).

In June 2015 when the onset of the magnetic storm was three-step (lines S1-S3 in Fig. 5, *b*; 6, *b*), already after the arrival of the second shock wave at Earth (line S2) the blackouts began in the Pevek, Norilsk, and Amderma ionosondes (Figure 6, *b*). During the main phase of the June 2015 magnetic storm there was no data in all the ionosondes, except for Zhigansk (see Figure 6, *b*), whose data clearly demonstrated the effect of the development of a negative ionospheric storm, i.e. a decrease in f_oF2 .

After the magnetic storms reached the maximum intensity (lines M1 in Figures 5, *a*, *b* and 6, *a*, *b*), in early recovery phases there was a sharp decrease in f_oF2 for both storms. This is clearly seen from the location of the points in the plots of variations relative to the daily average level of f_oF2 under quiet conditions. For the March 18–19, 2015 storm, the recorded values of f_oF2 were lower than the daily average level of f_oF2 under quiet conditions by more than 2 MHz for the ionosondes in Zhigansk and Norilsk. There were large data gaps for the ionosondes in Salekhard, Lovozero, and Sodankylä on March 18–19, 2015 (see Figures 5, *a*; 6, *a*), it is therefore impossible to figure out how much the f_oF2 values had changed. Complete radio signal blackouts occurred at night when the probability of formation of ionization troughs is high. For the highest-latitude ionosonde in Pevek, the period of decreased f_oF2 , and hence the electron density at the maximum F2-layer height, lasted almost until March 25, 2015 with a small increase in ionization on March 19, 2015.

For the June 2015 storm, the blackout of VS data was observed for all ionosondes of the high-latitude chain during most of the day on June 23, 2015. Measurements were also absent in ionosondes in Pevek, Amderma, Lovozero, and Sodankylä for another part of the day on June 24, 2015. Ionosonde data in Zhigansk, Norilsk, and Salekhard appeared at night in local time

on June 24.

From March 20, 2015, the ionospheric parameters began to recover to quiet day values observed before the storm, except for the highest-latitude ionosonde in Pevek. An isolated increase in magnetic activity on March 22, 2015, associated with the impact of CH HSS on Earth's magnetosphere (line M2 in Figure 5, *a*), did not cause a significant reaction in ionosonde measurements.

Noteworthy are periods of a significant increase in daytime ionization according to ionosonde data: March 27 in Norilsk; March 21–23, 27 in Salekhard; March 23, 27 in Amderma; March 23 in Lovozero; March 23 in Sodankylä. Those days, maximum daily f_oF2 values were to 9–10 MHz (marked with ovals in Figure 5, *a*), which exceeds by 2–3 MHz near-noon f_oF2 on quiet days of March 15–16, 2015 before the storm. Of special note is the general tendency for daily average f_oF2 to increase. According to the data from the same ionosondes (in Norilsk, Salekhard, Amderma, Lovozero, and Sodankylä), after March 25, 2015 nighttime ionization increased (minimum f_oF2 rose from 2–3 MHz to ~4 MHz).

During the June 2015 storm, ionospheric ionization began to recover in late afternoon on June 24. The increase in the intensity of the June 25 geomagnetic storm again to the level of a weak storm, caused by CME after the M6/2b solar flare on June 22, once more led to a short period of blackouts in ionosondes in Pevek, Zhigansk, Salekhard, Amderma, and Lovozero. By July 3, 2015, the overall ionization level in the region, where the high-latitude ionosonde chain is located, had not recovered to the quiet level before the storm onset. It is clearly seen that there is a negative trend in temporal variations of f_oF2 (red line in Figure 5, *b*) relative to daily average f_oF2 under quiet conditions (black line in Figure 5, *b*).

DISCUSSION OF THE RESULTS OF EXPERIMENTAL DATA ANALYSIS

An important role in atmosphere and ionosphere physics of the high-latitude Eurasian region under study belongs to its geographical location on Earth's surface and orientation relative to the Sun. Figure 2, *b* shows the location of the ionosondes relative to the 66°33' N latitude of the Arctic Circle. The ionosondes in Zhigansk, Salekhard, and Sodankylä are seen to be approximately at this latitude; the remaining ionosondes in Pevek, Norilsk, Amderma, and Lovozero are located at higher latitudes. This is especially important for analyzing events occurring near the summer and winter solstices because they occur during the polar day or night.

The measurement data from all ionosondes of the Eurasian high-latitude chain (Figures 5, 6) under quiet conditions (before the magnetic storms), as well as under disturbed geomagnetic conditions, convincingly confirm the characteristic features of ionization of the high-latitude ionosphere obtained by the local empirical model of electron density from the Norilsk DPS-4 digisonde data [Ratovsky et al., 2013], describing daily and seasonal variations, as well as solar cycle variations.

Maximum daily f_oF2 in March under quiet conditions before the storm (Figures 5, *a*; 6, *a*) is significantly higher than in June (Figures 5, *b*; 6, *b*). Minimum night f_oF2 in June (Figures 5, *b*; 6, *b*) exceeds minimum f_oF2 in March (Figures 5, *a*; 6, *a*). Diurnal variations of f_oF2 during the summer solstice have only one near-noon maximum (Figures 5, *b*; 6, *b*) as in the equinox (Figures 5, *a*; 6, *a*).

The increases in ionospheric ionization over the high-latitude regions of Eastern, Western Siberia and Europe (ovals in Figure 5, *a*) and the associated trend of increasing average daily f_oF2 (except for the ionosonde in Zhigansk) during the analyzed period on March 17–30, 2015 (red lines in Figure 5, *a*) might have been caused by large-scale disturbances of thermospheric molecular gas. Notice that from March 21, 2015 the geomagnetic activity level, according to Dst and PCN , was already undisturbed ($Dst > -50$ nT, $PCN < 2$ mV/m) (Figure 1, *a*). After the isolated increase in magnetic activity on March 22, 2015 (from 06:00–09:00 to ~18 UT), associated with the impact of CH HSS on Earth's magnetosphere, from March 23, 2015 the geomagnetic situation was already quiet until the end of the analyzed period on March 30.

Figure 7 exhibits a sequence of maps of global spatial distributions of the density ratio $[O]/[N_2]$ in the thermosphere above ~100 km, derived from GUVI TIMED satellite measurements in the Northern Hemisphere for each day on March 16–27, 2015 [<http://guvitimed.jhuapl.edu/guvi-gallery13on2>]. Unfortunately, the satellite data for the period considered is limited to ~65° N. The day-to-day evolution of these global maps allows us to visually analyze the formation and dynamics of large-scale regions of low $[O]/[N_2]$ in the high and middle latitudes of the Northern Hemisphere. Having formed in the polar regions of the thermosphere, this wave-like disturbance then propagates to midlatitudes and transforms in space and time for several days during the storm recovery phase. Due to the high frequency of molecular ion-neutral collisions, such a wave acquires a large scale and momentum and moves over considerable distances even when the magnetospheric source is "turned off" in auroral latitudes as in our case. The physical parameter $[O]/[N_2]$ is one of the key parameters determining the state of the ionosphere—thermosphere system during ionospheric storms. A decrease in $[O]/[N_2]$ in thermospheric gas causes the electron density in this region to decrease and

hence the negative ionospheric storm effect to develop.

Analysis carried out in [Chernigovskaya et al., 2019; Chernigovskaya et al., 2021] has shown that a vast region of low $[O]/[N_2]$ was formed in the lower thermosphere over the Far East (see Figure 7) during the main phase of the March 17, 2015 magnetic storm. This wave-like disturbance, which covered the entire territory of high-latitude Eurasia and huge areas of midlatitudes (to 30° N), moved westward over the territory of Eastern and Western Siberia toward Europe for about four days (to March 20, 2015) during the magnetic storm recovery phase. As a result, a prolonged negative ionospheric storm effect was observed in the mid-latitude ionosphere over Eurasia at F2-region heights till March 20, 2015 (Figures 5, *a*; 6, *a*).

From March 21, the intensity of the region of low $[O]/[N_2]$ in the thermosphere was decreasing. Coverage of mid-latitude territories decreased (see Figure 7). The region covered by low $[O]/[N_2]$ changed little in space from day to day. The geomagnetic situation was already quiet by this time (see Figure 1, *a*). The increase in magnetic activity on March 22, 2015 led to a slight intensification of the region of low $[O]/[N_2]$ on March 22–23, mainly over the regions of high and middle latitudes of the Western Hemisphere: North America, the Pacific Ocean, and the Far East since these regions were in the night and dusk sectors. The territory of high-latitude Eastern and Western Siberia (ionosondes in Norilsk, Salekhard, Amderma) on March 22, 2015 was in the region of higher $[O]/[N_2]$ (ovals in Figure 7). On March 23, 2015, the region of high $[O]/[N_2]$ expanded westward to the European region (ionosondes in Lovozero and Sodankylä). On March 22–23, 2015, the ionosonde measurements in Salekhard, Amderma, Lovozero, and Sodankylä showed higher f_oF2 (ovals in Figure 5, *a* and 7). The same situation occurred on March 27 for ionosondes in Norilsk, Salekhard, Amderma (Figures 5, *a* and 7). Significant spatio-temporal variations in the neutral composition of the thermosphere caused ionospheric electron density variations, recorded by the chain of high-latitude ionosondes. As a result, in these longitudes of Eurasia the negative phase of the ionospheric storm during the main and recovery phases of the March 2015 magnetic storm was changed by a positive disturbance of the ionospheric electron density after the geomagnetic disturbance.

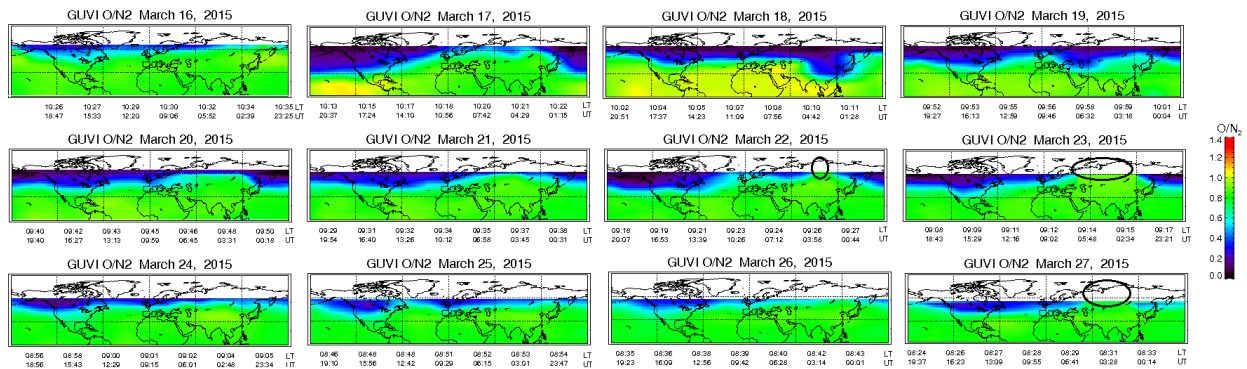


Figure 7. Maps of global spatial distributions of $[O]/[N_2]$ at ionospheric heights above ~100 km according to GUVI TIMED satellite measurements in the Northern Hemisphere for each day on March 16–27, 2015

Maps in Figure 7 show significant longitude differences in the global spatial distribution of $[O]/[N_2]$ in the thermosphere between the Eastern and Western hemispheres during the magnetic storm in March 2015. There was a region of low $[O]/[N_2]$ with minor spatio-temporal variations over the Western Hemisphere almost all the time. Variations in $[O]/[N_2]$ were observed over the Eastern Hemisphere from very low during the magnetic storm main and recovery phases to increased after the magnetic disturbance.

In [Chernigovskaya et al., 2020; Chernigovskaya et al., 2021], longitude variations in TEC data have been analyzed from measurements made at mid- and high-latitude chains of dual-frequency phase GPS/GLONASS receivers during extreme storms in March and June 2015. According to the geographical location, the chains of GPS/GLONASS receivers coincide well with the chains of ionosondes in Eurasia. However, the chains of GPS/GLONASS receivers cover not only the mainland of Eurasia and North America but also part of the islands in the oceans, which allows us to examine the global spatial and temporal picture of the development of ionospheric disturbances along latitudinal circles in the middle and high latitudes.

According to the results obtained in [Chernigovskaya et al., 2020; Chernigovskaya et al., 2021], in the North American sector the effect of the negative ionospheric storm in March 2015 was observed much longer than over Eurasia. Regions of low ionization persisted in the Western Hemisphere in middle and high latitudes for 7–8 days after the storm began. Over Eastern, Western Siberia and Europe in the Eastern Hemisphere, according to TEC data, ionospheric ionization recovered after the negative disturbance in 3–4 days and a region of increased ionization was formed in the F2-region at both middle and high latitudes. These results discussed above are perfectly confirmed by the measurement data from high-latitude ionosondes (Figures 5, *a*; 6, *a*).

The increase in ionospheric ionization (f_oF_2) over the vast region of Siberia and Europe on March 22–23 and March 27, 2015 with an excess of the f_oF_2 level for quiet days before the onset of the magnetic disturbance can be considered as a visible manifestation of the after-effect of magnetic storms [Klimenko et al., 2018].

Numerical calculations with the Global Self-consistent Model of the Thermosphere, Ionosphere, and Protonosphere (GSM TIP) [Namgaladze et al., 1988; Klimenko et al., 2018] as well as statistical analysis of data from mid-latitude ionosondes in Irkutsk and Kaliningrad have shown that the cause of positive electron density perturbations in the daytime a few days after the start of the magnetic storm recovery phase may be an increase in the concentration of atomic oxygen due to its transfer from equatorial to middle latitudes in the late recovery phase [Klimenko et al., 2018]. In turn, this transfer is determined by an additional neutral gas pressure gradient from low to high latitudes, resulting from the appearance of excessive neutral gas density at low latitudes in the geomagnetic storm main phase due to the transfer of oxygen from auroral latitudes toward the

equator. In this case, ionization values may exceed the level of quiet days before the magnetic disturbance. The authors compare the perturbation of $[O]/[N_2]$, as well as the electron density perturbation, with the oscillations of a pendulum that passes from a negative phase to a positive one within a few days after the start of the storm recovery phase.

The June extreme magnetic storm caused the effect of a strong negative ionospheric storm in the high-latitude ionosphere. Even ten days after the onset of the magnetic storm on July 3, 2015, the ionospheric ionization level was below the daily average level of f_oF_2 on quiet days before the storm (black line in Figure 5, *b*). These results, obtained from measurements of ionosondes of the high-latitude chain, are perfectly confirmed by the results of TEC analysis from the data acquired at the high-latitude chain of dual-frequency phase GPS/GLONASS receivers [Chernigovskaya et al., 2020; Chernigovskaya et al., 2021].

The different ionospheric response to geomagnetic storms, which is observed in this study, may also be attributed to the different probability of the occurrence of ionospheric storm positive or negative phases in different seasons of the year [Burešová et al., 2007]. In summer, the occurrence of only a negative effect during the entire magnetic storm main and recovery phases may be more probable. A confirmation of this is the visible effect of the negative ionospheric storm for the June 2015 event (see Figure 5, *b*). The transition from one type of storm effects to another is more typical for winter than for summer. Moreover, the probability of such behavior increases with decreasing latitude. For storms during the equinox, this relationship is not clear-cut. During the equinox in March 2015, we can see the initial effect of the positive ionospheric storm in the daytime after SSC with a sharp transition to the negative ionospheric storm during the magnetic storm main and recovery phases (see Figure 5, *a*) as a reaction of ionospheric ionization to an intense geomagnetic disturbance. Later, from March 22–23, 2015, the electron density tends to increase. There are daytime maxima of f_oF_2 exceeding the maximum daily values under quiet conditions before the storm, as well as an increase in night ionization (minimum f_oF_2 increased by 1–2 MHz).

In this study, the question arises again about the duration of the analyzed period of the ionospheric storm as a response of the ionosphere to a strong magnetic storm. Adjustments should be made to the traditional approach to the time interval of analysis of strong geomagnetic disturbances when the analysis ends at $Dst \geq 0$ [Chernigovskaya et al., 2021]. The results of this study once again confirm the conclusion that the ionospheric effects of strong magnetic storms should be examined on a time scale for several days after the magnetic storm since disturbed active regions of thermospheric gas continue to move westward by inertia and cause variations in electron density along the propagation path. For the March 2015 storm, the ionospheric effects, observed after the onset of the magnetic storm on March 17, 2015, still developed until the end of the analyzed time

period on March 30, 2015, although Dst from March 21, 2015 was already above the storm level ($Dst > -50$ nT); and after March 25, 2015, $Dst \geq 0$ (see Figure 1, a).

CONCLUSIONS

This work is a logical and very relevant sequel to our previous studies of spatio-temporal variations in ionospheric parameters over Eurasia in the mid-latitude region under quiet and disturbed geomagnetic conditions. For a comprehensive study of spatial-temporal features of ionospheric irregularities from radiophysical measurement data, to the analysis we have added measurement data from a chain of high-latitude ionosondes located in the north of the Eurasian continent at the latitude of the Arctic Circle and at higher latitudes. Using data from the Eurasian high-latitude ionosondes, we have analyzed features of the longitudinal-temporal variations in ionization of the high-latitude ionosphere during extreme magnetic storms of solar cycle 24 in March and June 2015, and have formulated the following results.

1. The special analysis we have carried out gave grounds to conclude that it is impossible to simultaneously use the parameters $h_m F2$ and $h'F2$ under conditions of increased geomagnetic activity. Therefore, for the comparative analysis of the electron density in the F2-region based on data from ionosondes of the high-latitude chain, we have employed (and will use in the future) only the parameter f_oF2 .

2. Noteworthy are significant differences in the nature of temporal variations in f_oF2 for the analyzed periods of magnetic storms. These differences (for example, the diurnal peak-to-peak amplitude of f_oF2 variations) are probably related to the characteristic features of the seasonal and diurnal variations in the background high-latitude ionosphere of this geographic region.

3. During the magnetic storm main and recovery phases, periods of ionosonde radio signal blackouts were observed which are associated with the combined action of mechanisms for the drop in ionization at heights of the upper ionosphere (negative ionospheric storms) and an abnormal increase in radio wave absorption at heights of the lower ionosphere due to penetration of energetic particles from the magnetosphere into the high-latitude ionosphere along magnetic field lines during magnetic disturbances.

4. During the extreme magnetic storms in March and June 2015 there were longitude differences in the nature of the ionospheric response to geomagnetic disturbances in the high-latitude region of Eurasia. This is probably due to seasonal features of the probability of occurrence of a positive or negative phase of an ionospheric storm in different seasons of the year. In summer, we can see a visible manifestation of the negative ionospheric storm for the June 2015 event. During the equinox, according to measurements of ionosondes in Norilsk, Salekhard, Amderma, Lovozero, Sodankylä, we observe a change in the initial effect of the positive ionospheric storm to the strong and prolonged negative one in the main and recovery phases of the magnetic storm as a response of ionospheric ionization to the intense geomagnetic disturbance in March 2015.

5. The longitude features of ionization variations in the high-latitude ionosphere over Eurasia, identified in this work, generally confirm the conclusions about spatio-temporal ionization variations in the mid-latitude region under disturbed geomagnetic conditions in March and June 2015, as derived from the data obtained at the chains of mid-latitude ionosondes and GPS/GLONASS receivers [Chernigovskaya et al., 2019, 2020; Chernigovskaya et al., 2021]. Detailed comparative analysis of the spatial-temporal features of variations in ionospheric parameters over mid- and high-latitude regions of Eurasia based on data from the chains of mid- and high-latitude ionosondes and GPS/GLONASS receivers during the extreme magnetic storm in March 2015 is presented in [Chernigovskaya et al., 2024].

6. The tendency for ionospheric ionization to increase over a vast region of Eastern, Western Siberia and Europe after the extreme magnetic storm in March 2015, according to measurements of the chain of high-latitude ionosondes, may be associated with the formation of high $[O]/[N_2]$ over this territory. Such an increase in ionospheric ionization with an excess of f_oF2 for quiet days before the onset of a magnetic disturbance can be considered as a vivid manifestation of the aftereffect of magnetic storms.

7. The results of this study once again confirm the conclusion that the ionospheric effects of strong magnetic storms should be examined on a time scale for several days after the end of a magnetic storm since the disturbed active regions of thermospheric gas continue to move westward by inertia and cause variations in electron density along the propagation path.

The work was financially supported by RSF (Project No. 23-27-00322)

The data from the ionosonde in Sodankylä, Finland was obtained from the UK Solar System Data Center [<https://www.ukssdc.ac.uk>]. The GUVI TIMED data used in this work is provided with the support of the NASA MO&DA program. The GUVI instrument was devised and built by the Aerospace Corporation and the Johns Hopkins University. The research supervisor is L.J. Paxton.

REFERENCES

- Alpatov V.V., Belyaev A.N., Kunitsyn V.E. Tomography methods in research and monitoring of the upper atmosphere and ionosphere. *Mir izmerenii* [Measurements World]. 2013, no. 2, pp. 31–37. (In Russian).
- Afraimovich E.L., Perevalova N.P. *GPS-monitoring verknei atmosfery Zemli* [GPS Monitoring of the Earth's Upper Atmosphere]. Irkutsk, 2006, pp. 90–94. (In Russian).
- Afraimovich E.L., Astafyeva E.I., Demyanov V.V., Edemskiy I.K., Gavrilyuk N.S., Ishin A.B., et al. A review of GPS/GLONASS studies of the ionospheric response to natural and anthropogenic processes and phenomena. *J. Space Weather and Space Climate*. 2013, vol. 3, no. A27. DOI: [10.1051/swsc/2013049](https://doi.org/10.1051/swsc/2013049).
- Andreeva E.S., Padokhin A.M., Nazarenko M.O., Tumanova Yu.S., Kalashnikova S.A. Tomographic methods for studying the atmosphere and near-Earth space: Current status and development prospects. *Trudy XXVII Vserossiiskoi otkry-*

- toi nauchnoi konferentsii "Rasprostraneniye radiovoln" [Proc. XXVII National Open Scientific Conference "Radio Wave Propagation"]. Kaliningrad, 2021, pp. 86–98. (In Russian).
- Buonsanto M.J. Ionospheric storms — a review. *Space Sci. Rev.* 1999, vol. 88, pp. 563–601.
- Burešová D., Laštovička J., De Franceschi G. Manifestation of strong geomagnetic storms in the ionosphere above Europe. *Space Weather*. Springer, 2007, pp. 185–202.
- Chernigovskaya M.A., Shpynev B.G., Khabituev D.S., Ratovskii K.G., Belinskaya A.Yu., Stepanov A.E., et al. Longitudinal variations of geomagnetic and ionospheric parameters during severe magnetic storms in 2015. *Sovremennyye problemy distantsionnogo zondirovaniya Zemli iz kosmosa* [Current Problems in Remote Sensing of the Earth from Space]. 2019, vol. 16, no. 5, pp. 336–347. DOI: [10.21046/2070-7401-2019-16-5-336-347](https://doi.org/10.21046/2070-7401-2019-16-5-336-347). (In Russian).
- Chernigovskaya M.A., Shpynev B.G., Yasyukevich A.S., Khabituev D.S. Ionospheric longitudinal variability in the Northern Hemisphere during magnetic storm from the ionosonde and GPS/GLONASS data. *Sovremennyye problemy distantsionnogo zondirovaniya Zemli iz kosmosa* [Current Problems in Remote Sensing of the Earth from Space]. 2020, vol. 17, no. 4, pp. 269–281. DOI: [10.21046/2070-7401-2020-17-4-269-281](https://doi.org/10.21046/2070-7401-2020-17-4-269-281). (In Russian).
- Chernigovskaya M.A., Shpynev B.G., Yasyukevich A.S., Khabituev D.S., Ratovsky K.G., Belinskaya A.Yu., et al. Longitudinal variations of geomagnetic and ionospheric parameters in the Northern Hemisphere during magnetic storms according to multi-instrument observations. *Adv. Space Res.* 2021, vol. 67, no. 2, pp. 762–776. DOI: [10.1016/j.asr.2020.10.028](https://doi.org/10.1016/j.asr.2020.10.028).
- Chernigovskaya M.A., Shpynev B.G., Khabituev D.S., Ratovsky K.G., Belinskaya A.Yu., Stepanov A.E., Bychkov V.V., Grigorieva S.A., Panchenko V.A., Mielich J. Studying the response of the mid-latitude ionosphere of the Northern Hemisphere to magnetic storms in March 2012. *Solar-Terr. Phys.* 2022, vol. 8, iss. 4, pp. 44–54. DOI: [10.12737/stp-84202204](https://doi.org/10.12737/stp-84202204).
- Chernigovskaya M.A., Yasyukevich A.S., Khabituev D.S. Ionospheric longitudinal variability in the Northern Hemisphere during magnetic storms in March 2012 from ionosonde and GPS/GLONASS data. *Solar-Terr. Phys.* 2023, vol. 9, iss. 4, pp. 99–110. DOI: [10.12737/stp-94202313](https://doi.org/10.12737/stp-94202313).
- Chernigovskaya M.A., Ratovsky K.G., Setov A.G., Khabituev D.S., Kalishin A.S., Stepanov A.E., et al. Ionospheric response over the high and middle latitude regions of Eurasia according to ionosonde data during the severe magnetic storm in March 2015. *Solar-Terr. Phys.* 2024, vol. 10. (In print).
- Cherniak I., Krankowski A., Zakharenkova I. Observation of the ionospheric irregularities over the Northern Hemisphere: Methodology and service. *Radio Sci.* 2014, vol. 49, no. 8, pp. 653–662. DOI: [10.1002/2014RS005433](https://doi.org/10.1002/2014RS005433).
- Chernyshov A.A., Chugunin D.V., Mogilevskii M.M., Moiseenko I.L., Kostrov A.V., Gushchin M.E., et al. Studying the inhomogeneous structure of the ionosphere using simultaneous measurements by CubeSat nanosatellites. *Izv. vuzov. Priborostroeniye* [J. Instrument Engineering]. 2016, vol. 59, no. 6, pp. 443–449. DOI: [10.17586/0021-3454-2016-59-6-443-449](https://doi.org/10.17586/0021-3454-2016-59-6-443-449). (In Russian).
- Deminov M.G. Electromagnetic and plasma processes from the interior of the Sun to the interior of the Earth. *Yubileinyi sbornik IZMIRAN-75* [Anniversary Collection IZMIRAN-75]. Moscow, 2015, pp. 295–346. (In Russian).
- Deminov M.G., Shubin V.N. Empirical model of the location of the main ionospheric trough. *Geomagnetism and Aeronomy*. 2018, vol. 58, no. 3, pp. 348–355. DOI: [10.1134/S0016793218030064](https://doi.org/10.1134/S0016793218030064).
- Enell C.-F., Kozlovsky A., Turunen T., Ulich T., Väitalo S., Scotto C., Pezzopane M. Comparison between manual scaling and Autoscala automatic scaling applied to Sodankylä Geophysical Observatory ionograms. *Geoscientific Instrumentation, Methods and Data Systems*. 2016, no. 5, pp. 53–64. DOI: [10.5194/gi-5-53-2016](https://doi.org/10.5194/gi-5-53-2016).
- Huang X., Reinisch B.W. Vertical electron density profiles from digisonde ionograms. The average representative profile. *Annali di Geofisica*. 1996, vol. XXXIX, no. 4, pp. 751–756.
- Hunsucker R.D., Hargreaves J.K. The High-Latitude Ionosphere and Its Effects on Radio Propagation. Cambridge University Press, New York, 2003, 617 p.
- Jakowski N. Radio occultation techniques for probing the ionosphere. *The Radio Science Bull.* 2005, no. 314, pp. 4–15.
- Kalishin A.S., Blagoveshchenskaya N.F., Troshichev O.A., Frank-Kamenetskii A.V. AARI: Geophysical Research in High Latitudes. *Polyarnye issledovaniya* [Polar Investigations]. 2020, no. 3-4 (107-108), pp. 60–74. DOI: [10.22204/2410-4639-2020-106-107-3-4-60-78](https://doi.org/10.22204/2410-4639-2020-106-107-3-4-60-78). (In Russian).
- Karpachev A.T. Dynamics of main and ring ionospheric troughs at the recovery phase of storms/substorms. *J. Geophys. Res.* 2021, no. 126, e2020JA028079. DOI: [10.1029/2020JA028079](https://doi.org/10.1029/2020JA028079).
- Karpachev A.T., Klimenko M.V., Klimenko V.V. Longitudinal variations of the ionospheric trough position. *Adv. Space Res.* 2019, vol. 63, iss. 2, pp. 950–966. DOI: [10.1016/j.asr.2018.09.038](https://doi.org/10.1016/j.asr.2018.09.038).
- Klimenko M.V., Klimenko V.V., Despirak I.V., Zakharenkova I.E., Kozlov B.V., Cherniakov S.M., et al. Disturbances of the thermosphere-ionosphere-plasmasphere system and auroral electrojet at 30° E longitude during the St. Patrick's Day geomagnetic storm on 17–23 March 2015. *J. Atmos. Solar-Terr. Phys.* 2018, vol. 180, pp. 78–92. DOI: [10.1016/j.jastp.2017.12.017](https://doi.org/10.1016/j.jastp.2017.12.017).
- Kozlovsky A., Turunen T., Ulich T. Rapid-run ionosonde observations of traveling ionospheric disturbances in the auroral ionosphere. *J. Geophys. Res.* 2013, vol. 118, pp. 5265–5276.
- Krinberg I.A., Tashchilin A.V. Ionosfera i plazmosfera [Ionosphere and Plasmasphere]. Moscow, Nauka Publ., 1984, 188 p. (In Russian).
- Kunitsyn V.E., Padokhin A.M., Kurbatov G.A., Yasyukevich Yu.V., Morozov Yu.V. Ionospheric TEC estimation with the signals of various geostationary navigational satellites. *GPS Solutions*. 2016, vol. 20, pp. 877–884. DOI: [10.1007/s10291-015-0500-2](https://doi.org/10.1007/s10291-015-0500-2).
- Loewe C.A., Prölss G.W. Classification and mean behavior of magnetic storms. *J. Geophys. Res.* 1997, vol. 102, no. A7, pp. 14,209–14,213.
- MacDougall J.W., Grant I.F., Shen X. The Canadian advanced digital ionosonde: design and results. *WDC A for Solar-Terrestrial Physics, Report UAG-104*. Boulder, Colorado, USA, 1995, pp. 21–27.
- Mamrukov A.P., Khalipov V.L., Filippov L.D., Stepanov A.E., Zikrach E.K., Smirnov V.F., Shestakova L.V. Geophysical information on oblique radio reflections at high latitudes and their classification. *Issledovaniya po geomagnetizmu, aehronomii i fizike Solntsa* [Research on Geomagnetism, Aeronomy and Solar Physics]. 2000, vol. 111, pp. 14–27. (In Russian).
- Matsushita S. A study of the morphology of ionospheric storms. *J. Geophys. Res.* 1959, vol. 64, no. 3, pp. 305–321. DOI: [10.1029/JZ064i003p00305](https://doi.org/10.1029/JZ064i003p00305).
- Mikhailov A.V. Ionospheric F2-layer storms. *Física de la Tierra*. 2000, vol. 12, pp. 223–262.
- Namgaladze A.A., Korenkov Yu.N., Klimenko V.V., Karpov I.V., Bessarab F.S., Surotkin V.A., et al. Global model of the thermosphere-ionosphere-protonosphere system. *Pure and Applied Geophysics*. 1988, vol. 127, no. 2-3, pp. 219–254.
- Perevalova N.P., Romanova E.B., Tashchilin A.V. Detec-

tion of high-latitude ionospheric structures using GNSS. *J. Atmos. Solar-Terr. Phys.* 2020, vol. 207, 105335. DOI: [10.1016/j.jastp.2020.105335](https://doi.org/10.1016/j.jastp.2020.105335).

Polyakov V.M., Shchepkin L.A., Kazimirovsky E.S., Korkourov V.D. *Ionosfernye protsessy* [Ionospheric Processes]. Novosibirsk, Nauka Publ., 1968, 535 p. (In Russian).

Ratovsky K.G., Oinats A.V., Medvedev A.V. Regular features of the polar ionosphere characteristics from digisonde measurements over Norilsk. *Adv. Space Res.* 2013, vol. 51, pp. 545–553. DOI: [10.1016/j.asr.2011.09.026](https://doi.org/10.1016/j.asr.2011.09.026).

Stepanov A.E., Khalipov V.L., Golikov I.A., Bondar' E.D. *Polyarizatsionnyi dzhety: uzkie i bystrye dreify subavroral'noi ionosfernoi plazmy* [Polarization jet: narrow and fast drifts of subauroral ionospheric plasma]. Yakutsk, SVFU Publ., 2017, 176 p. (In Russian).

Themens D.R., Jayachandran P.T., Galkin I., Hall C. The Empirical Canadian High Arctic Ionospheric Model (E-CHAIM): N_mF_2 and h_mF_2 . *J. Geophys. Res. Space Phys.* 2017, vol. 122, pp. 9015–9031. DOI: [10.1002/2017JA024398](https://doi.org/10.1002/2017JA024398).

Troshichev O.A., Sormakov D.A. PC index as a proxy of the solar wind energy that entered into the magnetosphere: 3. Development of magnetic storms. *J. Atmos. Solar-Terr. Phys.* 2018, vol. 180. DOI: [10.1016/j.jastp.2017.10.012](https://doi.org/10.1016/j.jastp.2017.10.012).

Tumanova Yu.S., Andreeva E.S., Nesterov I.A. Observations of an ionospheric trough over Europe at different levels of geomagnetic disturbance based on radio tomography data. *Uchenye zapiski fizicheskogo fakulteta Moskovskogo universiteta* [Moscow University Physics Bulletin]. 2016, no. 3, p. 163906. (In Russian).

Vystavnoi V.M., Makarova L.N., Shirochkov A.V., Egorova L.V. Research of the high-latitude ionosphere by vertical sounding using a modern digital ionosonde CADI. *Geliogeofizicheskie issledovaniya* [Heliogeophysical Res.] 2013, vol. 4, pp. 1–10. (In Russian).

URL: <http://wdc.kugi.kyoto-u.ac.jp> (accessed December 20, 2023).

URL: <https://www.ngdc.noaa.gov> (accessed January 15, 2024).

URL: <https://www.swpc.noaa.gov/noaa-scales-explanation> (accessed January 15, 2023).

URL: www.solen.info/solar/old_reports (accessed December 20, 2023).

URL: <https://wdc.kugi.kyoto-u.ac.jp/wdc/Sec3.html> (accessed December 20, 2023).

URL: http://www.wdcb.ru/stp/geomag/geomagn_PC_ind_ru.html (accessed December 20, 2023).

URL: https://www.ukssdc.ac.uk/wdcci/iono_menu.html (accessed December 20, 2023).

URL: http://icenter.izmiran.ru/f-h_db.php (accessed November 23, 2023).

URL: <http://guvitimed.jhuapl.edu/guvi-gallery13on2> (accessed February 5, 2024).

URL: <https://www.ukssdc.ac.uk> (accessed December 20, 2023).

Original Russian version: Chernigovskaya M.A., Setov A.G., Ratovsky K.G., Kalishin A.S., Stepanov A.E., published in *Solnechnozemnaya fizika*. 2024. Vol. 10. Iss. 2. P. 38–52. DOI: [10.12737/szf-102202404](https://doi.org/10.12737/szf-102202404). © 2023 INFRA-M Academic Publishing House (Nauchno-Izdatelskii Tsentr INFRA-M)

How to cite this article

Chernigovskaya M.A., Setov A.G., Ratovsky K.G., Kalishin A.S., Stepanov A.E. Variability of ionospheric ionization over Eurasia according to data from a high-latitude ionosonde chain during extreme magnetic storms in 2015. *Solar-Terrestrial Physics*. 2024. Vol. 10. Iss. 2. P. 34–47. DOI: [10.12737/stp-102202404](https://doi.org/10.12737/stp-102202404).